

Status of atmospheric ν_μ oscillations and decoherence after the first K2K spectral data

G.L. Fogli,¹ E. Lisi,¹ A. Marrone,¹ and D. Montanino²

¹ Dipartimento di Fisica and Sezione INFN di Bari
Via Amendola 173, 70126 Bari, Italy

² Dipartimento di Scienza dei Materiali and Sezione INFN di Lecce
Via Arnesano, 73100 Lecce, Italy

Abstract

We review the status of ν_μ flavor transitions of atmospheric neutrinos in the 92 kton-year data sample collected in the first phase of the Super-Kamiokande (SK) experiment, in combination with the recent spectral data from the KEK-to-Kamioka (K2K) accelerator experiment (including 29 single-ring muon events). We consider a theoretical framework which embeds flavor oscillations plus hypothetical decoherence effects, and where both standard oscillations and pure decoherence represent limiting cases. It is found that standard oscillations provide the best description of the SK + K2K data, and that the associated mass-mixing parameters are determined at $\chi^2 = 1$ (and $N_{DF} = 1$) as: $m^2 = (2.6 \pm 0.4) \cdot 10^{-3} \text{ eV}^2$ and $\sin^2 2\theta = 1.00^{+0.00}_{-0.05}$. As compared with standard oscillations, the case of pure decoherence is disfavored, although it cannot be ruled out yet. In the general case, additional decoherence effects in the ν_μ channel do not improve the fit to the SK and K2K data, and upper bounds can be placed on the associated decoherence parameter. Such indications, presently dominated by SK, could be strengthened by further K2K data, provided that the current spectral features are confirmed with higher statistics. A detailed description of the statistical analysis of SK and K2K data is also given, using the so-called "pull" approach to systematic uncertainties.

PACS numbers: 14.60.Pq, 13.15.+g, 03.65.Yz, 95.55.Vj

I. INTRODUCTION

In its first phase of operation (years 1996-2001), the Super-Kamiokande (SK) experiment has provided, among other important results, compelling evidence for atmospheric disappearance [1, 2]. This evidence, now firmly based on a high-statistics 92 kton-year exposure [3], has not only been corroborated [4] by consistent indications in the MACRO [5] and Soudan 2 [6] atmospheric neutrino experiments, but has also been independently checked by the first long-baseline K2K-to-Kamioka (K2K) accelerator experiment [7, 8], using SK as a target for ν 's produced 250 km away with $E_{\text{beam}} = 1.3 \text{ GeV}$.

Neutrino flavor oscillations, originated by non-zero mass-mixing parameters ($m^2; \sin^2 2\theta$) in the ν channel, provide by far the best and most natural (and probably unique) explanation for the observed disappearance [1, 2]. Among the "exotic" scenarios which have been proposed as radical alternatives (see [2, 4, 9, 10] for reviews), at present only hypothetical neutrino decoherence [11] (see also [12, 13]) appears as a possible "survivor" in the official SK data analysis [4, 14, 15]. All the other models envisaged so far to challenge the standard picture are strongly rejected as dominant explanations, and are bound to give at most subdominant effects (see, e.g., [2, 4, 9]).

In this paper, we review the phenomenological status of both standard oscillations and decoherence effects in the ν channel, in the light of the latest SK atmospheric zenith distributions of leptons [3, 4, 16] and of the first spectral results from the K2K experiment [8, 16]. In Sec. II we briefly review the adopted theoretical framework and describe the data set used. In Sec. III and IV we show, respectively, the results of our analysis for the cases of standard oscillations and pure decoherence, while in Sec. V we consider the most general case (oscillation+decoherence). Conclusions are given in Sec. VI.

We find that standard oscillations provide the best fit to the SK+K2K data, and that the mass-mixing parameters are determined at 1 σ as

$$m^2 = \text{eV}^2 = (2.6 \pm 0.4) \cdot 10^{-3}; \quad (1)$$

$$\sin^2 2\theta = 1.00^{+0.00}_{-0.05}; \quad (2)$$

with errors scaling linearly, with good accuracy, up to 3σ . Conversely, possible additional decoherence effects are generally disfavored, although not very strongly. We discuss how the upper bounds on such effects, currently dominated by SK, can potentially be improved by further K2K spectral data. The technical details of our SK and K2K data analysis are fully described in two appendices, using the so-called "pull" approach to systematic uncertainties.

II. THEORETICAL FRAMEWORK AND EXPERIMENTAL DATA

Oscillating neutrino systems may be thought as extremely sensitive interferometers with long arm lengths. When the interferometer beams interact with a background (e.g., matter), the interference pattern may be altered, and may even disappear if the background is "fuzzy." In theories of quantum gravity, it has long been speculated that the space-time itself may act as a "fuzzy" or "foamy" background for any propagating particle, leading to possible decoherence and dissipative phenomena on macroscopic scales (see, e.g., the bibliography in [11]). In this case, the neutrino evolution has to be described in the language of quantum open systems interacting with a generic environment [12, 13].

In Ref. [11] the formalism of quantum open systems has been applied to the case of two-family ν transitions of atmospheric neutrinos. Assuming entropy increase and energy

conservation in the neutrino subsystem, the evolution equation was shown to depend on only one additional (decoherence) parameter, here denoted as λ^2 , in addition to the usual mass-mixing parameters ($m^2; \sin^2 2\theta$)¹. With the further assumption of Lorentz-invariance of λ^2 , it was shown [11] that the survival probability takes, in natural units, the form

$$P(m^2; \lambda^2) = 1 - \frac{\sin^2 2\theta}{2} \left[1 - e^{-\frac{\lambda^2 L}{2E}} \cos \frac{m^2 L}{2E} \right]; \quad (3)$$

where E (L) is the neutrino energy (pathlength), and λ^2 has the dimensions of a squared mass. In the absence of first-principle calculations, λ^2 must be considered as a purely phenomenological parameter, to be constrained by experimental data.

The above equation has two interesting limits. The first is reached for $\lambda^2 = 0$, corresponding to the well-known case of standard oscillations,

$$P^{\text{osc}}(m^2; \lambda^2) = 1 - \frac{\sin^2 2\theta}{2} \left[1 - \cos \frac{m^2 L}{2E} \right]; \quad (4)$$

which perfectly fits atmospheric data with $m^2 \approx 3 \cdot 10^{-3} \text{ eV}^2$ and $\sin^2 2\theta \approx 1$. The second limit is reached for $\lambda^2 = 0$, corresponding to the case of pure decoherence

$$P^{\text{dec}}(\lambda^2; \lambda^2) = 1 - \frac{\sin^2 2\theta}{2} \left[1 - \exp \left(-\frac{\lambda^2 L}{2E} \right) \right]; \quad (5)$$

where the oscillation pattern is completely absent and the disappearance rate becomes monotonic in $L=E$. Surprisingly, the pure decoherence case turned out to fit well the 52 kton-year data SK atmospheric data for $m^2 \approx 3 \cdot 10^{-3} \text{ eV}^2$ and $\sin^2 2\theta \approx 1$, with a χ^2 comparable to the standard oscillation case [11]. Only with almost doubled SK statistics (92 kton-year exposure [3]) some weak indications have started to emerge against the pure decoherence scenario [4, 14, 15].

It is important to note that neutrino decay [17] can lead to an exponentially decreasing P qualitatively similar to Eq. (5). The decay and decoherence scenarios cannot thus be easily distinguished in the disappearance channel. However, they can be distinguished through the appearance mode, i.e., through neutral current (NC) events and appearance events in SK [3]. In fact, while in the decoherence case the total number of active neutrinos is conserved, in the decay scenario it decreases with $L=E$. The nonobservation of NC event suppression and the indications for appearance in SK can thus be used to reject decay [3, 4, 15] but not decoherence effects.

We remark that, in the general case [Eq. (3)], decoherence effects basically acts as a damping factor for the oscillating term [11, 18]. Testing atmospheric and long-baseline accelerator neutrino data through Eq. (3) amounts thus to test how well the oscillatory pattern is favored by (or hidden in) the data. Therefore, the decoherence scenario represents a useful benchmark, although its theoretical motivations are admittedly weaker than those supporting standard oscillations. In practice, in fits with unconstrained ($m^2; \lambda^2; \sin^2 2\theta$), the emergence of the standard oscillatory pattern should be signalled by a preference for small values of λ^2 . As we shall see, SK and K2K consistently favor $\lambda^2 \neq 0$; however, the absence of a clear oscillation pattern in the data makes this indication not very strong yet.

¹ The relation with the parameter λ in [11] is $\lambda^2 = 2\lambda$.

We conclude this section with a review of the SK and K2K data sets used for our analysis (see the appendices for more details). Concerning SK atmospheric neutrino data (92 kton-year [3, 4, 16]), we use the following zenith angle (θ_z) distributions of leptons: sub-GeV μ -like and e -like events (SG μ and SG e), divided in 10+10 bins; multi-GeV μ -like and e -like events (MG μ and MG e), divided in 10+10 bins; upward stopping and through-going events (US μ and UT μ), divided in 5+10 bins. The calculation of the theoretical events rates R_n^{theo} in each of the 55 bins is done as in [19, 20, 21]. The SK statistical analysis is considerably improved with respect to [19, 21], where only three sources of systematic errors were used (leading to correlated uncertainties in energy, angle, and flavor mis-identification [19]). Now the set of systematic errors has been enlarged to 11 entries, leading to a more complex structure of correlated errors affecting the R_n^{theo} 's, with allowance for various kinds of (relative) normalization and shape uncertainties. As emphasized in [22] for the solar neutrino case, systematic uncertainties can be implemented in the χ^2 statistics through two equivalent methods: 1) by building the total covariance matrix ("covariance method"), or 2) by adding quadratic penalties in the systematic pulls ("pull method"). The latter approach (adopted in this work) allows to study how systematic errors alter the theoretical predictions from the central values R_n^{theo} to "shifted" values $\overline{R}_n^{\text{theo}}$, in order to match the data. The difference $\overline{R}_n^{\text{theo}} - R_n^{\text{theo}}$ is thus useful to gauge the size and the direction of systematic effects in the data fit. More precise definitions and technical details are given in Appendix A.

Concerning the K2K data, we use the absolute spectrum of muon events in terms of the reconstructed neutrino energy E_μ [8, 16], which provides a total of 29 events (here divided in 6 bins). In this sample, the parent neutrino interactions are dominantly quasi-elastic (QE), and the reconstructed energy E_μ is thus closely correlated with the true neutrino energy E_ν .² In each bin, we attach to the theoretical prediction N_n^{theo} the two leading systematic errors (due to near-far and normalization uncertainties) through the pull approach. As for the SK analysis, we also discuss the systematically shifted theoretical predictions $\overline{N}_n^{\text{theo}}$. The relevant technical details are given in Appendix B.

III. STANDARD OSCILLATIONS

In this section we discuss updated bounds on the parameters $(\delta m^2; \sin^2 2\theta)$, governing the scenario of standard oscillations. The most important result is a significant strengthening of the upper bound on δm^2 induced by K2K data.

Figure 1 shows the joint bounds on the $(\delta m^2; \sin^2 2\theta)$ parameters from our analysis of SK, K2K, and SK+K2K data, derived through χ^2 cuts around the χ^2_{min} . The χ^2_{min} and their positions are reported in the "standard oscillation" columns of Table I. The global SK best fit ($\chi^2_{\text{min}} = 34.8$) might seem somewhat too good, as compared with the $N_{\text{DF}} = 55 - 2$ degrees of freedom. However, this value is only 1.8 below the typical χ^2 expectations ($N_{\text{DF}} - 2N_{\text{DF}}$), and is thus not suspicious from a statistical viewpoint.

In Fig. 1, the bounds in the left panel are very close to the official SK ones, as presented in [3, 4, 16]. The bounds in the middle panel are instead slightly weaker than the official K2K ones [8], especially in terms of $\sin^2 2\theta$. In particular, we do not find a lower bound

² We cannot use the full K2K data sample (56 events [8]), which contains 27 additional events of dominantly non-QE origin, whose analysis is basically not reproducible outside the K2K collaboration.

TABLE I: Coordinates and values of the absolute Δm^2 minima for separate and combined fits to SK and K2K data, in the scenarios of standard oscillation, pure decoherence, and oscillations plus decoherence.

Best fits	Standard oscillations			Pure decoherence			Oscillations plus decoherence		
	SK	K2K	SK + K2K	SK	K2K	SK + K2K	SK	K2K	SK + K2K
Δm^2 (eV ²)	$2.72 \cdot 10^{-3}$	$2.65 \cdot 10^{-3}$	$2.63 \cdot 10^{-3}$				$2.72 \cdot 10^{-3}$	$2.65 \cdot 10^{-3}$	$2.63 \cdot 10^{-3}$
$\sin^2 2\theta$	1.00	0.82	1.00	1.00	0.86	1.00	1.00	0.82	1.00
Δm^2 (eV ²)				$2.42 \cdot 10^{-3}$	$2.46 \cdot 10^{-3}$	$2.44 \cdot 10^{-3}$	0.00	0.00	0.00
Δm^2	34.8	9.4	45.2	42.1	11.5	54.1	34.8	9.4	45.2

on $\sin^2 2\theta$ at 99% C.L. (for $N_{DF} = 2$). The reason is that we cannot use the additional (dominantly) non-QE event sample of K2K (27 events), which would help to constrain the overall rate normalization and thus $\sin^2 2\theta$. This fact might also explain why we find the K2K best fit at $\sin^2 2\theta = 0.82$ rather than at 1.00 as in [8].³ Due to the slight anticorrelation between Δm^2 and $\sin^2 2\theta$ in the K2K analysis (middle panel of Fig. 1), an increase of $\sin^2 2\theta$ from 0.82 to 1.00 generates a slight decrease in the K2K favored range for Δm^2 , which is reflected in the SK+K2K best-fit Δm^2 (see Table I).

By comparing the left and right panels of Fig. 1, the main effect of K2K appears to be the strengthening of the upper bound on Δm^2 , consistently with the trend of the first K2K data (rate only [7], no spectrum) [21]. The main reason is that, for $\Delta m^2 \approx (4\text{--}6) \cdot 10^{-3} \text{ eV}^2$, the first oscillation minimum would be located at or just above the K2K energy spectrum peak, implying a strong local and overall suppression of the expected events, contrary to the K2K observations.

Figure 2 shows the SK and SK+K2K bounds on Δm^2 , when the $\sin^2 2\theta$ parameter is projected (minimized) away. The linear scale in Δm^2 makes the K2K impact on the upper limit more evident. Notice that, up to $\Delta m^2 \approx 3 \cdot 10^{-3} \text{ eV}^2$, the global (SK+K2K) χ^2 function is approximately parabolic in the linear variable Δm^2 , so that one can properly define a one-standard-deviation error for this parameter. This useful feature of the SK+K2K fit was already argued on the basis of a graphical reduction of the official SK and K2K likelihood functions [23], and is here confirmed through a full analysis. By keeping only the first significant figure in the error estimate, a parabolic fit provides the 1 σ range

$$\Delta m^2 = (2.6 \pm 0.4) \cdot 10^{-3} \text{ eV}^2; \quad (6)$$

with N errors scaling linearly with N (up to $N \approx 3$).⁴

The bounds on $\sin^2 2\theta$ are instead entirely dominated by SK. Figure 3 shows the χ^2 function in terms of $\sin^2 2\theta$, for Δm^2 projected (minimized) away in the SK fit. In this figure, the addition of K2K data would insignificantly change the bounds (not shown), which thus hold for both the SK and the SK+K2K fit. Also in this case, the nearly parabolic behavior of χ^2 allows to properly define a 1 σ range,

$$\sin^2 2\theta = 1.00^{+0.00}_{-0.05}; \quad (7)$$

³ In any case, this difference is not statistically significant, since the Δm^2 increase from our K2K best-fit point to maximum mixing is < 1 .

⁴ This range is consistent with the estimate $\Delta m^2 = (2.7 \pm 0.4) \cdot 10^{-3} \text{ eV}^2$ of [23], derived from a less detailed analysis.

with the lower N error scaling linearly with N (up to $N \sim 3$).⁵ Equations (6) and (7) concisely review the current fit to the standard oscillation parameters, as anticipated in the Introduction.

Figure 4 shows the comparison between observations and best-fit predictions for the SK zenith distributions. The best-fit point refers to the case of SK + K2K standard oscillations in Table I. Since the very good agreement between data and theory is no longer a surprise, in the following we comment on the "fine structure" of the SK data fit. This requires, however, that the reader can grasp the difference between theoretical predictions with and without the shifts induced by correlated systematics (solid and dashed histograms in Fig. 4, respectively), which is explained in detail in Appendix A.

In Fig. 4, the comparison between solid and dashed histograms shows that the systematic shifts are often comparable in size to the statistical errors, implying that just increasing the SK atmospheric statistics will hardly bring decisive new information on the standard oscillation scenario (or on physics beyond it). In the SG and MG samples, the fit clearly exploits the systematic uncertainties to increase the e-like event normalization, especially in the upward direction, so as to reduce the "electron excess" possibly indicated by SK data.⁶ Concerning $\bar{\nu}$ -like events in the SG and MG samples, the fit shows an opposite tendency to slightly decrease the normalization of (especially down-going) events. The tendency appears to be reversed in the high-energy UT sample. Taken together, these opposite shifts of e-like and $\bar{\nu}$ -like expectations in the SG and MG samples seem to suggest some systematic deviation from the predicted $\nu/\bar{\nu}$ ratio which, although not statistically alarming (see the last paragraph of Appendix A), should be kept in mind. In fact, deviations of similar size might have their origin in neutrino physics beyond 2 oscillations, e.g.: 1) subleading 3 oscillations, which could slightly increase the e-like event rates (see, e.g., [19, 20, 29]), or 2) subleading (short-baseline) $\nu/\bar{\nu}$ oscillations in the so-called (and still alive [30, 31]) $3+1$ scenario, which might slightly alter the down-going muon rates, as well as the front-detector K2K rate [32, 33, 34]. Unfortunately, since such effects are typically not larger than the systematic shifts in Fig. 4, they are likely (if any) to remain hidden in higher-statistics SK data, unless a significant reduction of the current systematics can be accomplished. The happy side of the story is that, for the same reasons, typical subleading effects beyond standard 2 oscillations do not significantly alter the fit results in Eqs. (6) and (7).

Figure 5 shows the comparison between data and theory for the K2K absolute spectrum of events, for the same oscillation best-fit point as in Fig. 4. In this case, the amount of systematic deviations preferred by the fit is much smaller than the current statistical error, implying that there is a great potential for improvements with higher K2K statistics.

IV. PURE DECOHERENCE (AND COMPARISON WITH OSCILLATIONS)

In this section we discuss the bounds on the parameters $(\theta^2; \sin^2 2\theta)$, governing the scenario of pure decoherence [Eq. 5]. We also discuss how this scenario compares with standard oscillations in fitting SK and K2K data.

⁵ The "upper" (null) error is, of course, trivial.

⁶ This tendency could be exacerbated by adopting the most recent atmospheric flux calculations, which consistently predict a lower normalization at relatively low energies [24, 25, 26, 27]. Nevertheless, preliminary results indicate that the induced changes in the $(\theta^2; \sin^2 2\theta)$ bounds would be minimal [28].

Figure 6 shows the joint bounds on the $(\theta^2; \sin^2 2\theta)$ parameters from our analysis of SK, K2K, and SK+K2K data, derived through χ^2 cuts around the χ^2_{\min} , as reported in the "pure decoherence" columns of Table I. Such bounds are clearly dominated by SK. The best-fit values of θ^2 are numerically close to the previous ones for θ^2 , since for both oscillations and decoherence one gets large disappearance effects for $xL=E \gg 0$ (1), where $x = \theta^2$ or m^2 [11].

The global SK+K2K best-fit for pure decoherence ($\chi^2_{\min} = 54.1$) is 9 units higher than for standard oscillations ($\chi^2_{\min} = 45.2$), where 7 units are provided by SK alone.⁷ On the one hand, this difference shows that the data start to have some sensitivity to decoherence effects, and tend to globally disfavor them. On the other hand, this sensitivity is not sufficient to claim rejection of such effects on a purely phenomenological basis. The features that tend to disfavor decoherence are better explained in terms of the best-fit theoretical distributions.

Figure 7 shows the SK zenith distributions for the global (SK+K2K) best-fit to pure decoherence (see Table I), and should be compared with the analogous Fig. 4 for the case of standard oscillations. The differences are hard to detect at first sight. In the decoherence case, the only noticeable difference is a slightly less pronounced suppression of the muon rates for increasing L , which leads to slightly less tilted distributions, as compared with standard oscillations. Notice also that the pure decoherence formula (5) implies $P^{\text{dec}}_{1=2} = 1$ always, while the standard oscillation formula (4) admits θ^2 as low as $P^{\text{osc}} = 0$, which can help to get a more efficient suppression (unless the limit of averaged oscillations is reached). The small differences in the upgoing muon distribution slopes are then responsible for the χ^2 difference between the two scenarios in SK. We do not expect that additional NC-enriched data in SK can add significant contributions to this difference, since (contrary to the decay scenario [17]) decoherence preserves the number of active neutrinos, as previously observed. Moreover, given the size of the systematic shifts in both Figs. 7 and 4, it seems to us that higher SK statistics will not be decisive to disentangle decoherence from oscillations. We conclude that SK tend to disfavor the pure decoherence hypothesis through its accurate measurements of the upgoing muon distribution shapes; however, there seems to be little room for significant improvements with longer SK exposure.

Figure 8 shows the K2K absolute spectrum of events for the global (SK+K2K) best-fit to pure decoherence (see Table I), to be compared with the analogous Fig. 5 for standard oscillations. The differences between the theoretical predictions in these two Figures are significant, although the large statistical error bars reduce their effect to a mere χ^2 difference between the oscillation and decoherence fits. The inequality $P^{\text{dec}}_{1=2} = 1$ is crucial to provide a slightly worse fit in the decoherence case, since it forbids a significant overall suppression, which can instead be more easily achieved with oscillations, particularly at low energy. Therefore, there is room for significant improvements in the discrimination of the two scenarios with higher K2K statistics, by looking at the low-energy part of the spectrum; in fact, a local rate suppression $< 1=2$ would definitely rule out the decoherence hypothesis.

Higher K2K statistics will also allow a less coarse binning in the spectrum analysis. For this reason, we show in Figs. 9 and 10 the unbinned K2K spectrum for representative cases of standard oscillations and pure decoherence, respectively (at maximal mixing). The two scenarios show increasing differences for decreasing energy in all cases. Moreover, within the standard scenario (Fig. 9), the spectrum shows rapid shape variation with θ^2 . A

⁷ The SK collaboration finds a larger difference ($\chi^2 = 10.5$ [4, 14, 15]) by using more data. Notice that pure decoherence satisfies the goodness-of-fit test [$\chi^2_{\min} = N_{\text{D.F.}} \gg 0$ (1)] in both fits (SK and ours).

judicious choice of binning, especially in the low-energy part of the spectrum, might thus enhance the K2K discrimination power in future data analyses, and might also improve the determination of m^2 in the standard oscillation case.

V. OSCILLATION PLUS DECOHERENCE

In this section we consider the general case of oscillations plus decoherence [Eq. (3)], in order to check whether subdominant (rather than dominant) decoherence effects can help the fit to the data. It turns out that, by leaving $(m^2; \sin^2 2\theta; \delta^2)$ free, the best fit is reached for $\delta^2 = 0$ for both SK, K2K, and SK + K2K, as reported in the last three columns of Table I. The corresponding joint bounds on the model parameters are shown in Fig. 11, through projections onto the three coordinate planes. Standard oscillations ($\delta^2 = 0$) and nearly maximal mixing are clearly favored. However, the pure decoherence limit ($m^2 = 0$) is still marginally allowed by the data. As discussed in the previous section, further K2K statistics might help to disfavor this limit with higher confidence.

Since $\delta^2 = 0$ is consistently preferred, it makes sense to derive upper bounds on δ^2 , by projecting away the other two parameters $(m^2; \sin^2 2\theta)$ in the fit. Figure 12 shows the results of this exercise, in terms of the function $\chi^2(\delta^2)$. The upper bound at 3 corresponds to $\delta^2 \lesssim 3 \cdot 10^3 \text{ eV}^2$. Values of δ^2 few 10^3 eV^2 are sufficiently low to be compatible (as remarked in [11]) with the non-observation of $\nu_e \rightarrow \nu_\tau$ appearance in CHORUS and NOMAD [35].

We conclude by observing that a really general "oscillation plus decoherence" scenario should be performed with (at least) three neutrino families, in order to incorporate also solar and reactor neutrino flavor transitions, and possibly other phenomenological constraints. Models of this kind would imply several new decoherence parameters, as well as nontrivial complications related to unavoidable matter effects. However, given the robust theoretical and phenomenological basis for standard oscillations, and the lack of signals in favor of decoherence effects (so far), a time-consuming analysis of such extended models is perhaps unwarranted at present. It could become interesting, however, if further K2K data, plus future long-baseline accelerator data, would fail to show a clear oscillation pattern.

VI. SUMMARY AND CONCLUSIONS

We have analyzed in detail the current SK atmospheric neutrino data and the first K2K spectral data, in order to review the status of standard $\nu_\mu \rightarrow \nu_\tau$ oscillations, as well as of a possible "rival" scenario based on neutrino decoherence. We have provided updated bounds for the standard oscillation parameters [Eqs. (1) and (2)], and have found no evidence for decoherence effects. However, the SK + K2K data are not accurate enough to rule out the pure decoherence case yet. The (currently weak) indications against such effects appear to be currently dominated by SK data, but the statistical analysis of the uncertainties reveals that K2K will lead further progress in this field, especially through higher-statistics tests of the low-energy spectrum bins. In conclusion, standard $\nu_\mu \rightarrow \nu_\tau$ oscillations are in good health, and seemingly no alternative scenario is able to provide a better fit to the SK + K2K data. However, the "second best" explanation of SK + K2K data (i.e., pure decoherence) is still statistically acceptable, and can provide a useful phenomenological benchmark to test the emergence of the still hidden standard oscillation pattern.

Acknowledgments

This work was in part supported by the Italian M IUR and INFN within the "Astroparticle Physics" research project. One of us (E.L.) would like to thank the Organizers of the Triangle meeting in Vienna, of the Christmas Workshop in Madrid, and of the NOON Workshop in Kanazawa where preliminary results from this work were presented for kind hospitality.

APPENDIX A : STATISTICAL ANALYSIS OF SK DATA

In this paper, the calculation of the SK zenith distributions of e-like and μ -like event rates is performed as described in previous works [19, 20, 21]. In the absence of oscillations, we normalize our absolute rates to the official 92 kTy SK estimates [3], which are currently based on the one-dimensional fluxes by Honda et al. [36] for all classes of events⁸.

Our SK statistical analysis, previously based on a simplified approach to error correlations [19], has been significantly improved in two aspects: 1) it has been made more consistent with the error estimates of the SK collaboration, as reported in [38] (see also [39, 40, 41]); and 2) it has been cast in a "pull" rather than "covariance" form, as advocated in [22] for solar neutrinos.

We remind that the "pull" approach to correlated systematic uncertainties (see [22] and references therein) amounts to shift the theoretical rate R_n^{theo} in the n -th bin through a set of deviations c_k^n , where c_k^n is the 1 σ error associated to the k -th source of systematics (in the present case, $k = 1; \dots; 11$), and the c_k 's are random variables,

$$R_n^{\text{theo}} \rightarrow R_n^{\text{theo}} = R_n^{\text{theo}} + \sum_{k=1}^{11} c_k^n c_k^k : \quad (\text{A } 1)$$

The χ^2 function is then obtained by minimization over the c_k 's,

$$\chi_{\text{SK}}^2 = \min_{\{c_k\}} \sum_{n=1}^{55} \left[\frac{R_n^{\text{theo}} - R_n^{\text{expt}}}{\sigma_n^{\text{stat}}} \right]^2 + \sum_{k,h=1}^{11} c_k [^{-1}]_{hk} c_h^5 ; \quad (\text{A } 2)$$

where σ_n^{stat} represent the statistical errors (or, in general, the quadratic sum of all uncorrelated errors) for the n -th bin. Notice that, with respect to the discussion in [22], we now give allowance for correlations $_{hk}$ of the systematic error sources.⁹ The above χ^2 function is exactly equivalent to build a quadratic form in the unshifted differences $(R_n^{\text{theo}} - R_n^{\text{expt}})$, with a covariance matrix defined as

$$\sigma_{nm}^2 = \sigma_n^{\text{stat}} \sigma_m^{\text{stat}} + \sum_{k,h=1}^{11} c_k^h c_h^k : \quad (\text{A } 3)$$

The minimization in Eq. (A 2) leads to a solvable set of linear equations in the c_k 's, whose solution \bar{c}_k can provide useful information on the role of systematic uncertainties in the fit

⁸ The one-dimensional fluxes by the Bartol group [37] are used by the SK collaboration for comparison with the default Honda fluxes.

⁹ In [22] all error sources were strictly independent, so that $_{hk} = \delta_{hk}$. Generalizing to $_{hk} \neq \delta_{hk}$ leads to the appearance of the inverse correlation matrix $[^{-1}]_{hk}$ in the last term of Eq. (A 2).

[22]. For instance, it can be interesting to study how much the best-fit shifted rates

$$\overline{R}_n^{\text{theo}} = R_n^{\text{theo}} + \sum_{k=1}^{55} \overline{c}_n^k \quad (\text{A } 4)$$

differ from the standard ones (R_n^{theo}), as a consequence of the systematic pulls \overline{c}_n^k .¹⁰ This valuable information would be lost in the covariance approach.

Our characterization of the 11 sources of SK uncertainties follows (or, at least, is inspired by) the detailed error description given in [38] (see also [39, 40, 41]). There is, however, one important difference, related to the fact that the SK analysis is based on Monte Carlo (MC) simulations, while ours is based on direct calculations of the lepton rates. More precisely, while in the SK official analysis the systematic uncertainties act as re-weighting factors for each MC event [38, 39, 40, 41], in our case they act directly on the observable rates R_n ($n = 1; \dots; 55$), and are thus completely characterized by the 55 \times 11 matrix \overline{c}_n^k .

Table II shows our numerical assignments for the \overline{c}_n^k 's (basically derived from [38]), interpreted as percentage errors of the R_n^{theo} values (with or without oscillations). The second row of Table II reports the notation of [38] for the same error sources, which we now discuss. The 1st systematic error source (δ) represents a 25% overall normalization uncertainty, due to at least two components: atmospheric flux normalization error (20%) [25] and cross section uncertainties (15%), added in quadrature [39]. The 2nd error source (α) is the "slope" uncertainty (5% [38]) in the atmospheric energy spectrum, leading to a $10^{0.05} \approx 1 + 12\%$ normalization change for a 1 "tilt" of the spectrum slope over one energy decade. Since the SG and UT parent neutrino spectra are separated by about two decades in energy, we take for them $\alpha_n^2 = -12\%$ and $+12\%$, respectively. The MG and US event samples have roughly intermediate energies between the SG and UT ones (on a $\log E$ scale), so we assign them $\alpha_n^2 = -4\%$ and $+4\%$, respectively. The 3rd and 4th error sources (δ_s and δ_m) are the overall flavor ratio uncertainties for the SG and MG samples, respectively. The relatively large ring-counting error in the MG sample makes δ_m greater than δ_s [38]. The 5th error source (β) is the relative normalization error between partially and fully contained (PC and FC) events, estimated as 10.5% [38]. Since only the MG sample contains PC events (57%), the total (FC+PC) change in the MG normalization is reduced to $0.57 \times 10.5\% \approx 6\%$, as indicated in Table II. The 6th error source (δ_u) is the normalization uncertainty of upgoing muon events (US and UT) with respect to lower-energy events, mainly due to the relative cross section uncertainties. The 7th error source (δ_t) gives further allowance for a normalization shift of the US event rate only, dominated by the track length cut uncertainty. The 8th and 9th error sources (δ_s and δ_m) allow a small up-down asymmetry (about 3% at 1 $^\circ$) in the SG and MG zenith distributions, due to geometric and instrumental uncertainties. The 10th error source (δ_f) allows a small horizontal/vertical ratio uncertainty (about 2%) in the zenith distributions of FC events with momentum > 0.4 GeV for both the SG and MG samples, mainly related to atmospheric flux calculation uncertainties [38]. This error is reduced by a factor of 2 in the SGe and SG samples, due to a $1=2$ component of low-momentum FC events which are unaffected by this uncertainty, since they lose memory of the neutrino direction. A similar δ_f error reduction applies to the MG sample, due to

¹⁰ We observe that the SK collaboration basically shows the shifted $\overline{R}_n^{\text{theo}}$'s in the best-fit plots, while we have graphically reported the unshifted R_n^{theo} 's in previous works [19, 20, 21]. For the sake of comparison, Fig. 4 and 7 in this paper show both representations.

TABLE II: Set of 11 systematic errors f_n^k generated by several sources ($k = 1; \dots; 11$) and affecting in different ways the binned rates of the SK zenith distribution ($n = 1; \dots; 55$). All errors are given as percentage fraction of the theoretical rate in each bin: $s_n^k = 100 \cdot c_n^k = R_n^{\text{theo}}$. The formal identification with the uncertainties ($\%$; $\%$; $\%$; $\%$; $\%$; $\%$; $\%$; $\%$; $\%$; $\%$; $\%$) of [38] is given in the 2nd row. See the text for further details.

bin n	event class	$[\cos \theta_z^{\text{min}}; \cos \theta_z^{\text{max}}]$ range	s_n^1 (%)	s_n^2 (%)	s_n^3 (%)	s_n^4 (%)	s_n^5 (%)	s_n^6 (%)	s_n^7 (%)	s_n^8 (%)	s_n^9 (%)	s_n^{10} (%)	s_n^{11} (%)
1	SGe	[1.0; 0.8]	25	12	3	0	0	0	0	2.7	0	+1.0	0
2	SGe	[0.8; 0.6]	25	12	3	0	0	0	0	2.1	0	+0.5	0
3	SGe	[0.6; 0.4]	25	12	3	0	0	0	0	1.5	0	0.0	0
4	SGe	[0.4; 0.2]	25	12	3	0	0	0	0	0.9	0	0.5	0
5	SGe	[0.2; 0.0]	25	12	3	0	0	0	0	0.3	0	1.0	0
6	SGe	[+0.0; +0.2]	25	12	3	0	0	0	0	+0.3	0	1.0	0
7	SGe	[+0.2; +0.4]	25	12	3	0	0	0	0	+0.9	0	0.5	0
8	SGe	[+0.4; +0.6]	25	12	3	0	0	0	0	+1.5	0	0.0	0
9	SGe	[+0.6; +0.8]	25	12	3	0	0	0	0	+2.1	0	+0.5	0
10	MGe	[+0.8; +1.0]	25	12	3	0	0	0	0	+2.7	0	+1.0	0
11	MGe	[1.0; 0.8]	25	4	0	4.6	0	0	0	0	2.7	+2.0	0
12	MGe	[0.8; 0.6]	25	4	0	4.6	0	0	0	0	2.1	+1.0	0
13	MGe	[0.6; 0.4]	25	4	0	4.6	0	0	0	0	1.5	0.0	0
14	MGe	[0.4; 0.2]	25	4	0	4.6	0	0	0	0	0.9	1.0	0
15	MGe	[0.2; 0.0]	25	4	0	4.6	0	0	0	0	0.3	2.0	0
16	MGe	[+0.0; +0.2]	25	4	0	4.6	0	0	0	0	+0.3	2.0	0
17	MGe	[+0.2; +0.4]	25	4	0	4.6	0	0	0	0	+0.9	1.0	0
18	MGe	[+0.4; +0.6]	25	4	0	4.6	0	0	0	0	+1.5	0.0	0
19	MGe	[+0.6; +0.8]	25	4	0	4.6	0	0	0	0	+2.1	+1.0	0
20	MGe	[+0.8; +1.0]	25	4	0	4.6	0	0	0	0	+2.7	+2.0	0
21	SG	[1.0; 0.8]	25	12	+3	0	0	0	0	2.7	0	+1.0	0
22	SG	[0.8; 0.6]	25	12	+3	0	0	0	0	2.1	0	+0.5	0
23	SG	[0.6; 0.4]	25	12	+3	0	0	0	0	1.5	0	0.0	0
24	SG	[0.4; 0.2]	25	12	+3	0	0	0	0	0.9	0	0.5	0
25	SG	[0.2; 0.0]	25	12	+3	0	0	0	0	0.3	0	1.0	0
26	SG	[+0.0; +0.2]	25	12	+3	0	0	0	0	+0.3	0	1.0	0
27	SG	[+0.2; +0.4]	25	12	+3	0	0	0	0	+0.9	0	0.5	0
28	SG	[+0.4; +0.6]	25	12	+3	0	0	0	0	+1.5	0	0.0	0
29	SG	[+0.6; +0.8]	25	12	+3	0	0	0	0	+2.1	0	+0.5	0
30	SG	[+0.8; +1.0]	25	12	+3	0	0	0	0	+2.7	0	+1.0	0
31	MG	[1.0; 0.8]	25	4	0	+4.6	+6	0	0	0	2.7	+1.0	0
32	MG	[0.8; 0.6]	25	4	0	+4.6	+6	0	0	0	2.1	+0.5	0
33	MG	[0.6; 0.4]	25	4	0	+4.6	+6	0	0	0	1.5	0.0	0
34	MG	[0.4; 0.2]	25	4	0	+4.6	+6	0	0	0	0.9	0.5	0
35	MG	[0.2; 0.0]	25	4	0	+4.6	+6	0	0	0	0.3	1.0	0
36	MG	[+0.0; +0.2]	25	4	0	+4.6	+6	0	0	0	+0.3	1.0	0
37	MG	[+0.2; +0.4]	25	4	0	+4.6	+6	0	0	0	+0.9	0.5	0
38	MG	[+0.4; +0.6]	25	4	0	+4.6	+6	0	0	0	+1.5	0.0	0
39	MG	[+0.6; +0.8]	25	4	0	+4.6	+6	0	0	0	+2.1	+0.5	0
40	MG	[+0.8; +1.0]	25	4	0	+4.6	+6	0	0	0	+2.7	+1.0	0
41	US	[1.0; 0.8]	25	+4	0	0	0	+9.2	+5.6	0	0	0	0
42	US	[0.8; 0.6]	25	+4	0	0	0	+9.2	+5.6	0	0	0	0
43	US	[0.6; 0.4]	25	+4	0	0	0	+9.2	+5.6	0	0	0	0
44	US	[0.4; 0.2]	25	+4	0	0	0	+9.2	+5.6	0	0	0	0
45	US	[0.2; 0.0]	25	+4	0	0	0	+9.2	+5.6	0	0	0	0
46	UT	[1.0; 0.9]	25	+12	0	0	0	+9.2	0	0	0	0	+1.8
47	UT	[0.9; 0.8]	25	+12	0	0	0	+9.2	0	0	0	0	+1.4
48	UT	[0.8; 0.7]	25	+12	0	0	0	+9.2	0	0	0	0	+1.0
49	UT	[0.7; 0.6]	25	+12	0	0	0	+9.2	0	0	0	0	+0.6
50	UT	[0.6; 0.5]	25	+12	0	0	0	+9.2	0	0	0	0	+0.2
51	UT	[0.5; 0.4]	25	+12	0	0	0	+9.2	0	0	0	0	0.2
52	UT	[0.4; 0.3]	25	+12	0	0	0	+9.2	0	0	0	0	0.6
53	UT	[0.3; 0.2]	25	+12	0	0	0	+9.2	0	0	0	0	1.0
54	UT	[0.2; 0.1]	25	+12	0	0	0	+9.2	0	0	0	0	1.4
55	UT	[0.1; 0.0]	25	+12	0	0	0	+9.2	0	0	0	0	1.8

the substantial presence of (undetected) PC events [38]. The 11th error source ($\%$) gives allowance for a horizontal/vertical ratio uncertainty in the UT sample, which is instead argued to be irrelevant in the US sample (see [38]). Finally, we remark that the SK analysis contains a further error source (so-called L=E uncertainty, 15% [38, 39, 40, 41]) that we do not implement in our analysis. In particular, we think that the spread in L should be more properly included through integration over the known neutrino path length distribution (i.e., over the neutrino production heights at different angles) rather than being interpreted

TABLE III: Correlation matrix ρ_{hk} of systematic error sources ($h, k = 1; \dots; 11$) in the SK analysis, as taken from [38].

	1	2	3	4	5	6	7	8	9	10	11
1	+ 1.00	0	0	0	0	0	0	0	0	0	0
2		+ 1.00	0	0	0	0	0	0	0	0	0
3			+ 1.00	+ 0.31	0.17	0.03	0	0	0	0	0
4				+ 1.00	0.34	0	0	0	0	0	0
5					+ 1.00	+ 0.58	0.17	0	0	0	0
6						+ 1.00	0.25	0	0	0	0
7							+ 1.00	0	0	0	0
8								+ 1.00	+ 0.62	0	0
9									+ 1.00	0	0
10										+ 1.00	0
11											+ 1.00

TABLE IV : Values of the SK systematic pulls \bar{f}_k at the global (SK + K2K) best-fit point for standard θ oscillations.

k	1	2	3	4	5	6	7	8	9	10	11
\bar{f}_k	+ 0.19	+ 0.22	1.05	0.99	0.53	0.03	0.12	0.99	0.82	+ 0.07	+ 0.01

as an additional uncertainty.¹¹ We also observe that, in general, a "L=E error" becomes meaningless in scenarios where P is not a function of $L=E$, but of L and E separately (as is the case, e.g., in the presence of matter effects).

The 11 systematic error sources listed in Table II are not necessarily independent. For instance, the horizontal/vertical ratio uncertainties s and m are largely due to common geometric and instrumental effects, and are thus expected to be positively correlated. On the other hand, cross section uncertainties (affecting in different ways quasi-elastic and deep-inelastic scattering events) can generate a "migration" of events from one class to another, thus inducing negative correlations among the corresponding normalization uncertainties.

Table III reports explicitly the correlation matrix ρ_{hk} among the SK systematics, as taken from the careful estimates in [38]. This matrix enters in the χ^2_{SK} definition of Eq. (A2).

Finally, Table IV reports the systematic SK pulls \bar{f}_k ($k=1; \dots; 11$) at the global (SK + K2K) best-fit for standard θ oscillations, which have been used to calculate the "shifted" theoretical rates in Fig. 4. They appear to be relatively small for any k . Therefore, the induced differences $\bar{R}_n^{\text{theo}} - R_n^{\text{theo}}$ between the solid and dashed histograms in Fig. 4 represent tolerable systematic shifts of "typical" size.

APPENDIX B: CALCULATION AND STATISTICAL ANALYSIS OF THE K2K SPECTRUM

In this appendix we describe our calculation of the K2K spectrum of events and our approach to the K2K statistical analysis.

¹¹ We understand that future SK atmospheric data analyses might indeed fully incorporate the spread of L , as derived from recent three-dimensional flux calculations (T. Kajita, private communication).

TABLE V : Set of systematic errors f_n^k generated by several sources ($k = 1; \dots; 7$), and affecting in different ways the binned rates of the K2K energy distribution ($n = 1; \dots; 6$). All errors are given as percentage fraction of the theoretical number of events N_n^{theo} in each bin: $s_n^k = 100 \cdot f_n^k = N_n^{\text{theo}}$. The energy interval and the experimental number of events N_n^{expt} are given in the second and third row, respectively. See the text for details.

n	E range (GeV)	N_n^{expt}	s_n^1	s_n^2	s_n^3	s_n^4	s_n^5	s_n^6	s_n^7
1	[0.0;0.5]	3	2.6	0	0	0	0	0	5.0
2	[0.5;1.0]	4	0	4.3	0	0	0	0	5.0
3	[1.0;1.5]	14	0	0	6.5	0	0	0	5.0
4	[1.5;2.0]	2	0	0	0	10.4	0	0	5.0
5	[2.0;2.5]	4	0	0	0	0	11.1	0	5.0
6	> 2.5	2	0	0	0	0	0	12.2	5.0

1. Calculation of the K2K spectrum

Our oscillation analysis of the K2K spectral data is based on 29 single-ring -like (1R) events [8], binned into 6 intervals of the reconstructed neutrino energy E . The experimental number of events N_n^{expt} in each bin is given in Table V, together with the corresponding systematic uncertainties (discussed below). The no-oscillation expectations correspond to a total of 42.5 events, as graphically derived from Fig. 2 in [8, 16]. This data sample contains mainly muons from quasi-elastic (QE) scattering $\mu + n \rightarrow \mu + p$.¹²

In principle, for QE scattering on neutrons at rest, the reconstructed neutrino energy E depends only on the muon kinematics [8],

$$E = \frac{m_n E_\mu - m_\mu^2/2}{m_n - E_\mu + p_\mu \cos \theta} : \quad (\text{B1})$$

However, a number of effects can produce significant deviations of E from the true neutrino energy E_ν , including nuclear effects (Fermi motion, Pauli blocking, proton re-scattering [42, 43, 44]), detection uncertainties (SK resolution in energy and angle [45, 46]), and contamination from non-QE events [47, 48]. Therefore, the reconstructed energy E is distributed around the true energy E_ν through a certain (normalized) probability distribution function $R(E; E_\nu)$. This function smears out the oscillation pattern and must thus be taken into account, at least approximately, in the K2K analysis.

Although the function $R(E; E_\nu)$ is not explicitly provided by the K2K Collaboration [8], its main features can be roughly recovered from other studies. In particular, $R(E; E_\nu)$ has been derived (for a SK-like detector) through numerical simulations in [42, 45]. It turns out that [42, 45]: 1) E is typically biased towards slightly lower values than E_ν (with $\langle E - E_\nu \rangle = b \sim \text{few } 10 \text{ MeV}$),¹³ and 2) the rms. difference $\langle E - E_\nu \rangle_{\text{rms}} = \sigma_E$ increases from zero (at $E_\nu \sim 0.2 \text{ MeV}$) up to a plateau $\sigma_E = E_\nu \sim 20\%$ [42, 45]. We approximately embed these features in a Gaussian p.d.f. of the kind

$$R(E; E_\nu) \sim \frac{1}{\sigma_E \sqrt{2\pi}} e^{-\frac{1}{2} \frac{(E - E_\nu + b)^2}{\sigma_E^2}} ; \quad (\text{B2})$$

¹² We do not use the additional 27 events forming the total K2K data sample (56 events), since the simulation of (dominantly) non-QE events is not possible without very detailed K2K experimental information.

¹³ Contamination from non-QE events also produces a bias b in the same direction [47].

where we take $b' = 0.05 \text{ GeV}$ for the bias parameter and

$$R(E; E') = \exp \left(-\frac{0.2 (E - E')^2}{0.08} \right) \quad (\text{B } 3)$$

for the energy reconstruction error $E - E'$ above $E' > 0.2 \text{ GeV}$ ($E - E' = 0$ otherwise). Although we do not include the more detailed features investigated in [42, 45] (e.g., asymmetric tails), the above function $R(E; E')$ appears to be good enough for our current analysis. A better treatment will be possible when a description of $R(E; E')$ (or of equivalent information) in K2K will be made publicly available.¹⁴

The E' -spectrum of events expected in the presence of oscillations is calculated as

$$\frac{dN^{\text{theo}}}{dE} = \int dE' S(E') R(E; E') P(E - E'); \quad (\text{B } 4)$$

where $S(E')$ is the unoscillated spectrum at the SK detector (in terms of the true neutrino energy). We find that, in the relevant energy range $E' \in [0.2; 3.25] \text{ GeV}$, the K2K spectrum $S(E')$ is well approximated by the simple function

$$S(E') = (E' - 0.2)^{3.25} E'; \quad (\text{B } 5)$$

where $\alpha = 1.0056$, $\beta = 3.144$, and E_R is given in GeV . The factor $\gamma = 0.7389$ is then fixed by the normalization constraint $\int dE' dE S(E') R(E; E') = 42.5$ for no oscillation. The reader is referred to Fig. 9 for representative theoretical spectra dN^{theo}/dE , with and without oscillations (at maximal mixing). Such spectra are in reasonable agreement with the corresponding K2K ones as shown in [50].

2. Statistical analysis of the K2K spectrum

We bin both the K2K theoretical spectrum dN^{theo}/dE and the experimental spectrum into six energy intervals (see Table V). The statistical analysis of the K2K absolute number of events fN_n^X , $g_{n=1,\dots,6}$ ($X = \text{theo}; \text{expt}$) is performed, in analogy with the previous Appendix, by shifting the predictions through a set of (7, in this case) systematic deviations

$$N_n^{\text{theo}} \rightarrow N_n^{\text{theo}} = N_n^{\text{theo}} + \sum_{k=1}^7 c_n^k; \quad (\text{B } 6)$$

which are then minimized away in the χ^2 . The only formal difference with respect to the SK data fit is the use of Poisson statistics, required to deal with small number of events:

$$\chi^2_{\text{K2K}} = \min_{f, g} \sum_{n=1}^6 \left[N_n^{\text{theo}} - N_n^{\text{expt}} + N_n^{\text{expt}} \ln \frac{N_n^{\text{theo}}}{N_n^{\text{expt}}} \right] + \sum_{k \neq 1}^7 \left[\frac{1}{2} \ln \frac{1}{c_k} \right]; \quad (\text{B } 7)$$

¹⁴ We also note that several issues related to the characterization of the $E - E'$ difference in QE and non-QE events are currently being re-examined, in the light of the accuracy needed to analyze higher-statistics data in the K2K and future low-energy accelerator neutrino experiments (see, e.g., [44, 48, 49]).

TABLE VI: Correlation matrix c_{hk} ($h, k = 1, \dots, 7$) of systematics in the K2K analysis. The nontrivial 6×6 block, related to near-far extrapolation uncertainties, is derived from [51]. The 7th systematic error (independent overall normalization) is assumed to be uncorrelated.

	1	2	3	4	5	6	7
1	+ 1.00	0.25	0	0	0	0	0
2		+ 1.00	0	0	0	0	0
3			+ 1.00	+ 0.08	0.04	0.20	0
4				+ 1.00	+ 0.79	+ 0.19	0
5					+ 1.00	+ 0.39	0
6						+ 1.00	0
7							+ 1.00

TABLE VII: Values of the K2K systematic pulls f_k at the global (SK + K2K) best-fit point for standard $\nu_\mu \rightarrow \nu_e$ oscillations.

k	1	2	3	4	5	6	7
f_k	+ 0.02	0.01	+ 0.29	0.70	+ 0.38	+ 0.24	+ 0.38

The minimization in Eq. (B7), which can be easily performed through linearization in the small parameters f_k , yields the best-fit systematic pulls f_k . The shifted theoretical predictions for the number of events in each bin read then

$$\overline{N}_n^{\text{theo}} = N_n^{\text{theo}} + \sum_{k=1}^7 f_k c_n^k : \quad (\text{B } 8)$$

In the systematic error budget, we include the following (dominant) error sources, for which one can find a detailed description in [51]. The near-far extrapolation procedure in K2K leads to six systematic errors ($k = 1, \dots, 6$) in each bin, with significant bin-to-bin correlations [51]. The overall normalization uncertainty adds a further 5% error ($k = 7$) with full correlation in each bin. The numerical values of the 17 systematics c_n^k and of the correlation matrix c_{hk} , as derived from [51], are reported in Tables V and VI, respectively. These values enter in the χ^2_{K2K} definition of Eq. (B7).

Finally, Table VII reports the K2K systematic pulls f_k ($k = 1, \dots, 7$) at the global (SK + K2K) best-fit for standard $\nu_\mu \rightarrow \nu_e$ oscillations, from which the "shifted" theoretical rates in Fig. 5 are calculated. All the pulls appear to be relatively small.

-
- [1] SK Collaboration, Y. Fukuda et al., "Evidence for oscillations of atmospheric neutrinos," Phys.Rev.Lett. 81, 1562 (1998) [hep-ex/9807003].
 - [2] T. Kajita and Y. Totsuka, "Observation of atmospheric neutrinos," Rev.Mod.Phys. 73, 85 (2001).
 - [3] SK Collaboration, M. Shiozawa et al., "Experimental results on atmospheric neutrinos in Super-Kamiokande-I," in Neutrino 2002, Proceedings of the 20th International Conference on Neutrino Physics and Astrophysics (Munich, Germany, 2002), to appear.
 - [4] E.T. Kearns, "Atmospheric neutrinos in 2002," in HQ & L 2002, Proceedings of the 6th International Workshop on Heavy Quarks and Leptons (Viterbo sul Mare, Salerno, Italy, 2002), Frascati Phys. Ser. 28, 413 (2002) [hep-ex/0210019].

- [5] MACRO Collaboration, M. Ambrosio et al., "Measurements in upward-going muons and sterile neutrino oscillations," *Phys. Lett. B* 517, 59 (2001); "Low-energy atmospheric muon neutrinos in MACRO," *Phys. Lett. B* 478, 5 (2000).
- [6] Soudan 2 Collaboration, W. W. Allison et al., "The atmospheric neutrino flavor ratio from a 3.9 fiducial kton-year exposure of Soudan 2," *Phys. Lett. B* 449, 137 (1999) [[hep-ex/9901024](#)].
- [7] K2K Collaboration, S. H. Ahn et al., "Detection of accelerator produced neutrinos at a distance of 250-km," *Phys. Lett. B* 511, 178 (2001) [[hep-ex/0103001](#)].
- [8] K2K Collaboration, M. H. Ahn et al., "Indications of neutrino oscillation in a 250 km long-baseline experiment," *Phys. Rev. Lett.* 90, 041801 (2003) [[hep-ex/0212007](#)].
- [9] S. Pakvasa and J. W. F. Valle, "Neutrino properties before and after KamLAND," contribution to a special issue of the Proceedings of the Indian National Academy of Sciences on "Neutrinos" [[hep-ph/0301061](#)].
- [10] S. Pakvasa, "Testing neutrino properties at long baseline experiments and neutrino factories," in NuFact '00, Proceedings of the 2nd International Workshop on Neutrino Factories based on Muon Storage Rings (Monterey, California, 2000), *Nucl. Instrum. Meth. A* 472, 413 (2000) [[hep-ph/0008193](#)].
- [11] E. Lisi, A. Marrone, and D. Montanino, "Probing possible decoherence effects in atmospheric neutrino oscillations," *Phys. Rev. Lett.* 85, 1166 (2000) [[hep-ph/0002053](#)].
- [12] F. Benatti and R. Floreanini, "Massless neutrino oscillations," *Phys. Rev. D* 64, 085015 (2001) [[hep-ph/0105303](#)]; "Open system approach to neutrino oscillations," *J. High Energy Phys.* 2, 032 (2000) [[hep-ph/0002221](#)].
- [13] A. M. Gago, E. M. Santos, W. J. Teves, and R. Zukanovich Funchal, "Quest for the dynamics of $\mu \rightarrow e$ conversion," *Phys. Rev. D* 63, 113013 (2001) [[hep-ph/0010092](#)]; see also, by the same authors, "Quantum dissipative effects and neutrinos: Current constraints and future perspectives," *Phys. Rev. D* 63, 073001 (2001) [[hep-ph/0009222](#)].
- [14] E. T. Keams, talk at the Conference "Neutrinos: Data, Cosmos, and Planck Scale," Kavli Institute for Theoretical Physics (Santa Barbara, California, 2003), available at www.kitp.ucsb.edu.
- [15] M. B. Smy, "Neutrino experiments with Super-Kamiokande," Proceedings of the 3rd Tropical Workshop on Particle Physics and Cosmology (San Juan, Puerto Rico, 2002), edited by J. F. Nieves and C. N. Leung, *AIP Conf. Proc.* Vol. 655 (Melville, New York, 2003), p. 20.
- [16] R. J. Wilkes, "New Results from Super-K and K2K," in SSI 2002, Proceedings of the 30th SLAC Summer Institute on Particle Physics (Menlo Park, California, 2002) [[hep-ex/0212035](#)].
- [17] V. D. Barger, J. G. Learned, P. Lipari, M. Lusignoli, S. Pakvasa, and T. J. Weiler, "Neutrino decay and atmospheric neutrinos," *Phys. Lett. B* 462, 109 (1999) [[hep-ph/9907421](#)].
- [18] T. Ohlsson, "Equivalence between neutrino oscillations and neutrino decoherence," *Phys. Lett. B* 502, 159 (2001) [[hep-ph/0012272](#)].
- [19] G. L. Fogli, E. Lisi, A. Marrone, and G. Scioscia, "Super-Kamiokande atmospheric neutrino data, zenith distributions, and three-flavor oscillations," *Phys. Rev. D* 59, 033001 (1999) [[hep-ph/9808205](#)].
- [20] G. L. Fogli, E. Lisi, and A. Marrone, "Super-Kamiokande atmospheric neutrinos: Status of subdominant oscillations," *Phys. Rev. D* 64, 093005 (2001) [[hep-ph/0105139](#)].
- [21] G. L. Fogli, E. Lisi, and A. Marrone, "Indications on neutrino oscillation parameters from initial KEK-to-Kamioka and current SK data," *Phys. Rev. D* 65, 073028 (2002) [[hep-ph/0110089](#)].

- [22] G.L. Fogli, E. Lisi, A.M. Marrone, D.M. Montanino and A. Palazzo, "Getting the most from the statistical analysis of solar neutrino oscillations," *Phys. Rev. D* **66**, 053010 (2002) [[hep-ph/0206162](#)].
- [23] G.L. Fogli, G. Lettera, E. Lisi, A.M. Marrone, A. Palazzo, and A. Rotunno, "Three-flavor solar neutrino oscillations with terrestrial neutrino constraints," *Phys. Rev. D* **66**, 093008 (2002) [[hep-ph/0208026](#)].
- [24] M. Honda, "The calculation of atmospheric neutrino flux," in *NOON '03, Proceedings of the 4th Workshop on Neutrino Oscillations and their Origin* (Kanazawa, Japan, 2003); available at www-sk.icrr.u-tokyo.ac.jp/noon2003.
- [25] T.K. Gaisser, "Atmospheric neutrino fluxes," in *Neutrino 2002, Proceedings of the 20th International Conference on Neutrino Physics and Astrophysics* (Munich, Germany, 2002), to appear [[hep-ph/0209195](#)].
- [26] M. Honda, T. Kajita, K. Kasahara, and S. Midorikawa, "Comparison of three-dimensional and one-dimensional schemes in the calculation of atmospheric neutrinos," *Phys. Rev. D* **64**, 053011 (2001) [[hep-ph/0103328](#)].
- [27] G. Battistoni, A. Ferrari, P. Lipari, T. Montanuli, P.R. Sala, and T. Rancati, "A three-dimensional calculation of atmospheric neutrino flux," *Astropart. Phys.* **12**, 315 (2000) [[hep-ph/9907408](#)].
- [28] K. Kaneyuki, "Determination of neutrino oscillation parameters with atmospheric neutrinos," in *NuInt '01, Proceedings of the 1st International Workshop on Neutrino Nucleus Interactions in the few GeV region* (Tsukuba, Japan, 2001), edited by J.G. Moron, M. Sakuda, and Y. Suzuki, *Nucl. Phys. B (Proc. Suppl.)* **112**, 24 (2002).
- [29] O.L. Peres and A.Yu. Smirnov, "Testing the solar neutrino conversion with atmospheric neutrinos," *Phys. Lett. B* **456**, 204 (1999) [[hep-ph/9902312](#)].
- [30] C. Giunti, "Last CPT-invariant hope for LSND neutrino oscillations," [[hep-ph/0302173](#)].
- [31] A. Strumia, "Interpreting the LSND anomaly: sterile neutrinos or CPT-violation or ...?," *Phys. Lett. B* **539**, 91 (2002) [[hep-ph/0201134 v4](#)].
- [32] C. Giunti and M. Laveder, "Large μ and e \rightarrow μ transitions in short-baseline experiments?," *J. of High Energy Phys.* **0102**, 1 (2001) [[hep-ph/0010009](#)].
- [33] O.L.G. Peres and A.Yu. Smirnov, "(3+1) spectrum of neutrino masses: A chance for LSND?," *Nucl. Phys. B* **599**, 3 (2001) [[hep-ph/0011054](#)].
- [34] M. Maltoni, T. Schwetz, and J.W.F. Valle, "Constraining (3+1) sterile neutrino schemes," *Phys. Lett. B* **518**, 252 (2001) [[hep-ph/0107150](#)].
- [35] K. Zuber, "Latest CHORUS and NOMAD results," in *Moriond '02, 37th Rencontres de Moriond on Electroweak Interactions and Unified Theories* (Les Arcs, France, 2002), to appear [[hep-ex/0206006](#)].
- [36] M. Honda, T. Kajita, K. Kasahara, and S. Midorikawa, "Calculation of the flux of atmospheric neutrinos," *Phys. Rev. D* **52**, 4985 (1995) [[hep-ph/9503439](#)].
- [37] V. Agrawal, T.K. Gaisser, P. Lipari, and T. Stanev, "Atmospheric neutrino flux above 1 GeV," *Phys. Rev. D* **53**, 1314 [[hep-ph/9509423](#)].
- [38] J. Kamada, "Detailed studies of neutrino oscillation with atmospheric neutrinos of wide energy range from 100 MeV to 1000 GeV in Super-Kamiokande," PhD thesis, University of Tokyo, 2002; available at www-sk.icrr.u-tokyo.ac.jp/doc/sk/pub.
- [39] A. Kobayashi, "Atmospheric neutrino oscillation analysis using FLUKA 3D flux and Super-Kamiokande data," PhD thesis, University of Hawaii, 2002; available at www-sk.icrr.u-tokyo.ac.jp/doc/sk/pub.

- [40] K. Ishihara, "Study of θ_{12} and θ_{13} neutrino oscillations with atmospheric neutrino data in Super-Kamiokande," PhD thesis, University of Tokyo, 1999; available at www-sk.icrr.u-tokyo.ac.jp/doc/sk/pub.
- [41] M. D. Messier, "Evidence for neutrino mass from observations of atmospheric neutrinos with Super-Kamiokande" PhD thesis, Boston University, 1999; available at www-sk.icrr.u-tokyo.ac.jp/doc/sk/pub.
- [42] A. Blondel, M. Campanelli, and M. Fechner, "Reconstruction of neutrino energy in a large water Cherenkov detector using lepton information," CERN-NUFACT-NOTE-112, available at molat.home.cern.ch/molat/neutrino/nfnotes.html.
- [43] C. W. Walter, "Quasi-elastic events and nuclear effects with the K2K Sci-Fi detector," in NuInt '01, Proceedings of the 1st International Workshop on Neutrino Nucleus Interactions in the few GeV region (Tsukuba, Japan, 2001), edited by J.G. Moron, M. Sakuda, and Y. Suzuki, Nucl. Phys. B (Proc. Suppl.) 112, 140 (2002).
- [44] C. W. Walter, "Nuclear effects on QE reconstruction in low-energy neutrino long-baseline experiments," in NuInt '02, Proceedings of the 2nd International Workshop on Neutrino Nucleus Interactions in the few GeV region (Irvine, California, 2002), available at www.psuci.edu/~nuint.
- [45] A. Blondel, M. Campanelli, and M. Fechner, "Energy measurement of quasi-elastics, unfolding detector and physics effects," in NuFACT '02, Proceedings of the 4th International Workshop on Neutrino Factories based on Muon Storage Rings (London, England, 2002), available at www.hep.ph.ic.ac.uk/NuFact02.
- [46] A. Blondel, M. Campanelli, and M. Fechner, "Study of the reconstruction of neutrino oscillation parameters using spectral information from a Cherenkov detector," CERN-NUFACT-NOTE-120, available at molat.home.cern.ch/molat/neutrino/nfnotes.html.
- [47] Y. Itow, "Study of neutrino interaction in the K2K and the JHF-Kamioka long baseline neutrino oscillation experiment," in NuInt '01, Proceedings of the 1st International Workshop on Neutrino Nucleus Interactions in the few GeV region (Tsukuba, Japan, 2001), edited by J.G. Moron, M. Sakuda, and Y. Suzuki, Nucl. Phys. B (Proc. Suppl.) 112, 3 (2002).
- [48] Y. Itow, "K2K E spectrum measurement and interaction model," in NuInt '02, Proceedings of the 2nd International Workshop on Neutrino Nucleus Interactions in the few GeV region (Irvine, California, 2002), available at www.psuci.edu/~nuint.
- [49] D. Casper, "Comparisons of simulated data samples," in NuInt '02, Proceedings of the 2nd International Workshop on Neutrino Nucleus Interactions in the few GeV region (Irvine, California, 2002), available at www.psuci.edu/~nuint.
- [50] Y. Oyama, "Present status of the K2K experiment," in Beyond the Desert '02, Proceedings of the 3rd Conference on Physics Beyond the Standard Model (Oulu, Finland, 2002), to appear; available at cupp.oulu.fi/beyond02.
- [51] T. Kobayashi, "Translation from Near to Far at K2K," in NuFACT '02, Proceedings of the 4th International Workshop on Neutrino Factories based on Muon Storage Rings (London, England, 2002), available at www.hep.ph.ic.ac.uk/NuFact02.

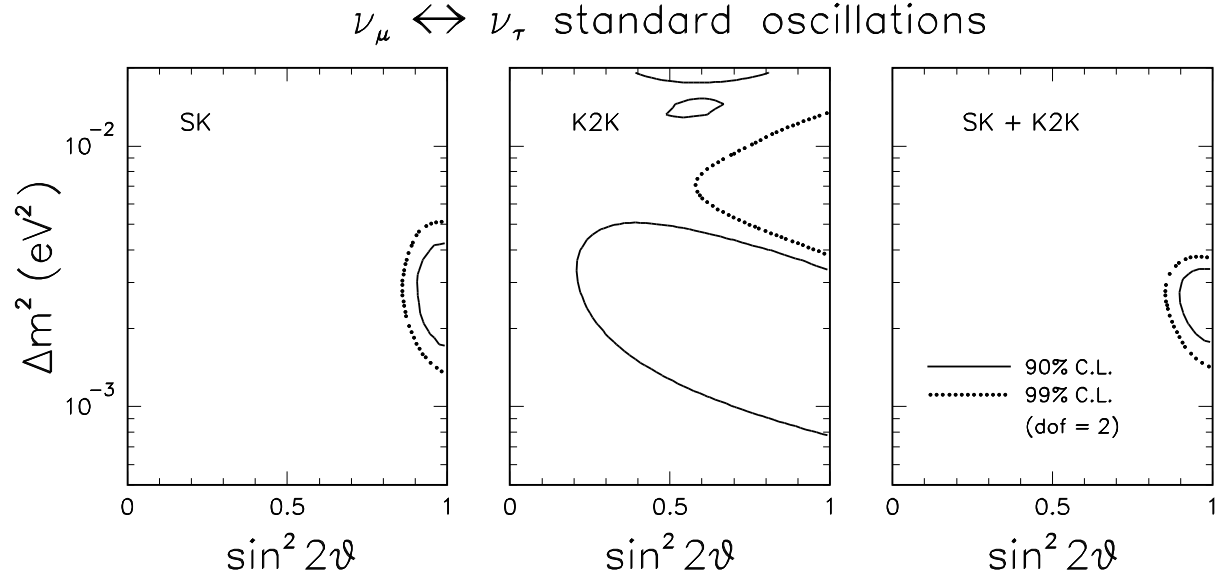


FIG. 1: Standard oscillations in the $\nu_\mu \leftrightarrow \nu_\tau$ channel: Bounds on the parameters (Δm^2 ; $\sin^2 2\theta$) from SK atmospheric data (left panel), K2K spectral data (middle panel), and their combination (right panel). The solid and dotted curves refer, respectively, to the 90% and 99% C.L. contours for $N_{\text{DF}} = 2$ ($\chi^2 = 4.61$ and 9.21).

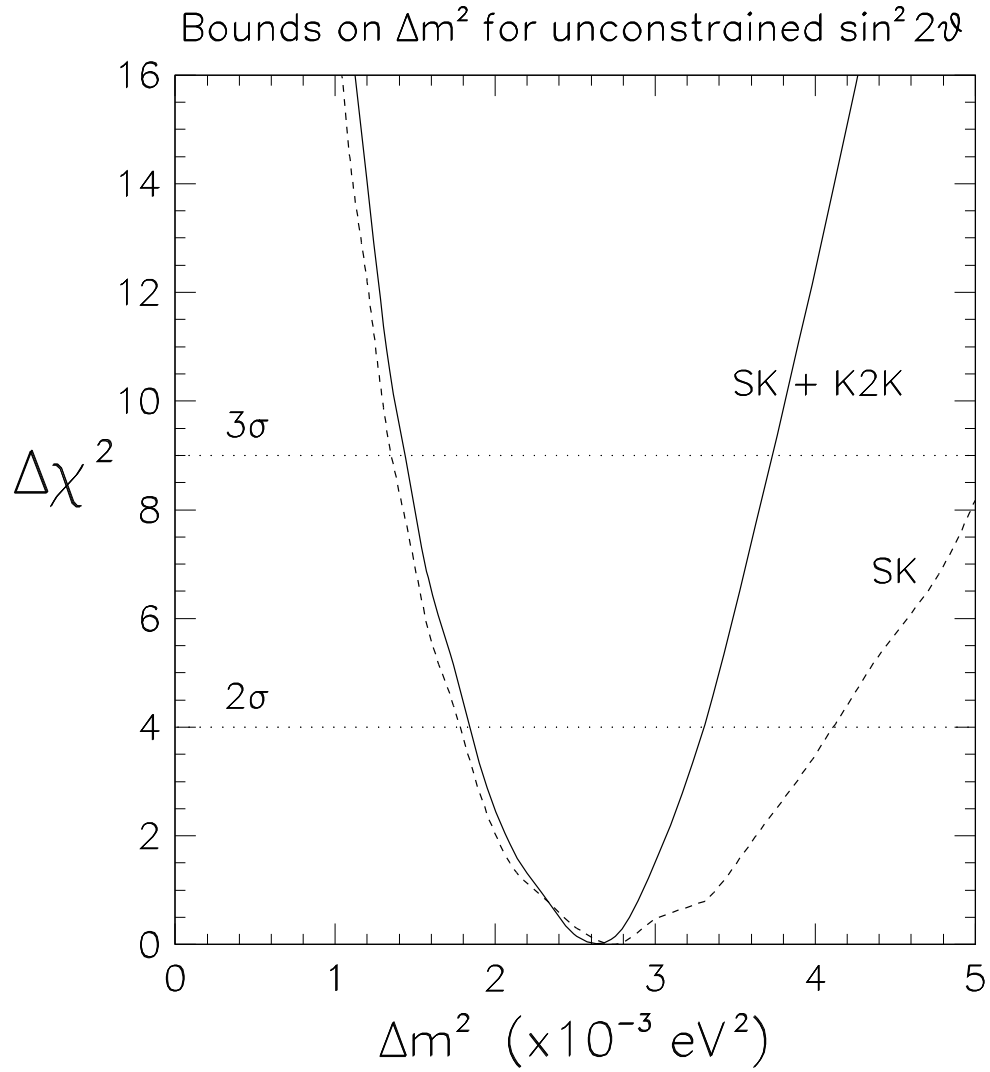


FIG. 2: Standard oscillations in the $\nu_\mu \rightarrow \nu_e$ channel: Bounds on Δm^2 for unconstrained $\sin^2 2\theta$ from SK (dashed curve) and SK + K2K (solid curve). The intersections with the horizontal dotted lines give the 2σ and 3σ (upper and lower) bounds on Δm^2 for $N_{DF} = 1$. By fitting the SK + K2K curve with a parabola, the 1σ interval is derived as $\Delta m^2 = (2.6 \pm 0.4) \times 10^{-3} \text{ eV}^2$.

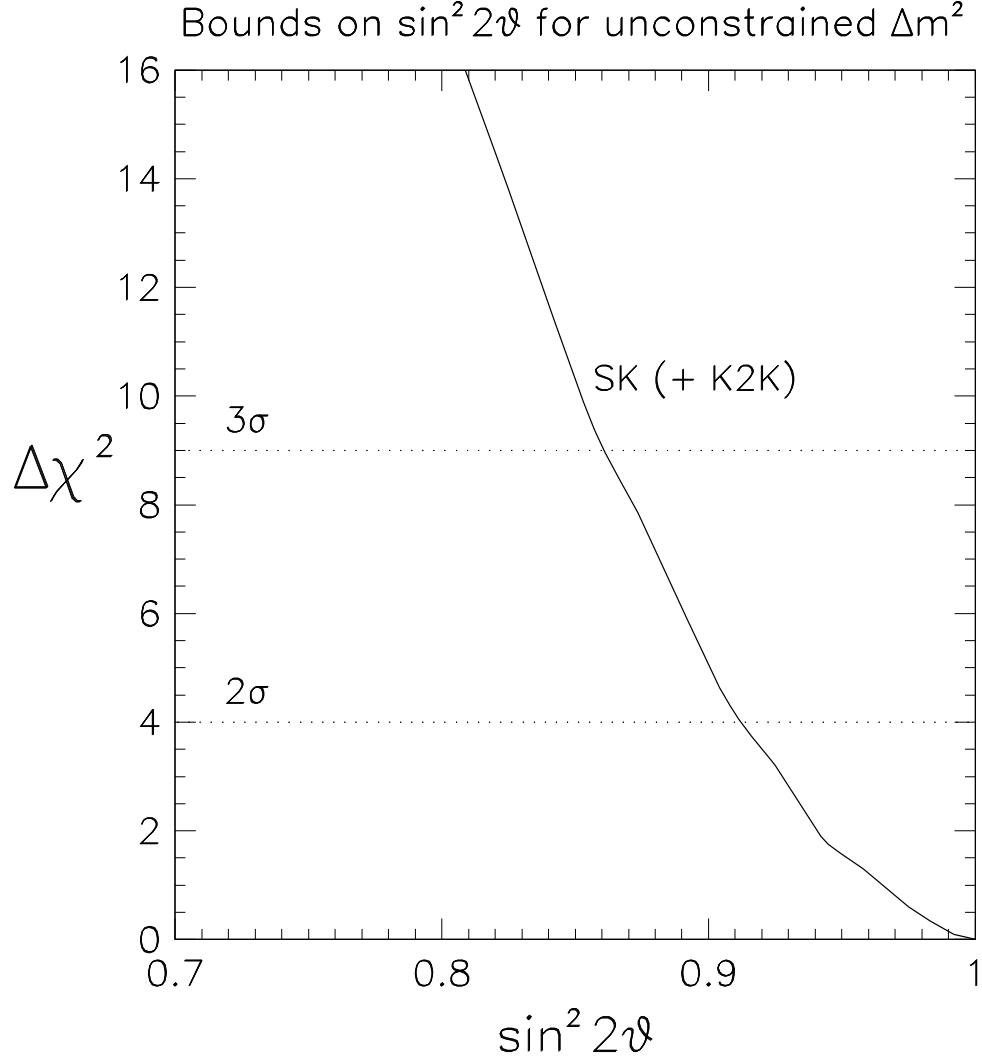


FIG. 3: Standard oscillations in the μ channel: Bounds on $\sin^2 2\vartheta$ for unconstrained m^2 from SK data. The inclusion of K2K data induces negligible changes (not shown). The intersections with the horizontal dotted lines give the 2 and 3 σ lower bounds on $\sin^2 2\vartheta$ for $N_{DF} = 1$. By fitting the curve with a parabola, the 1σ interval is derived as $\sin^2 2\vartheta = 1.00^{+0.00}_{-0.05}$, where only the first significant digit is kept in the lower error.

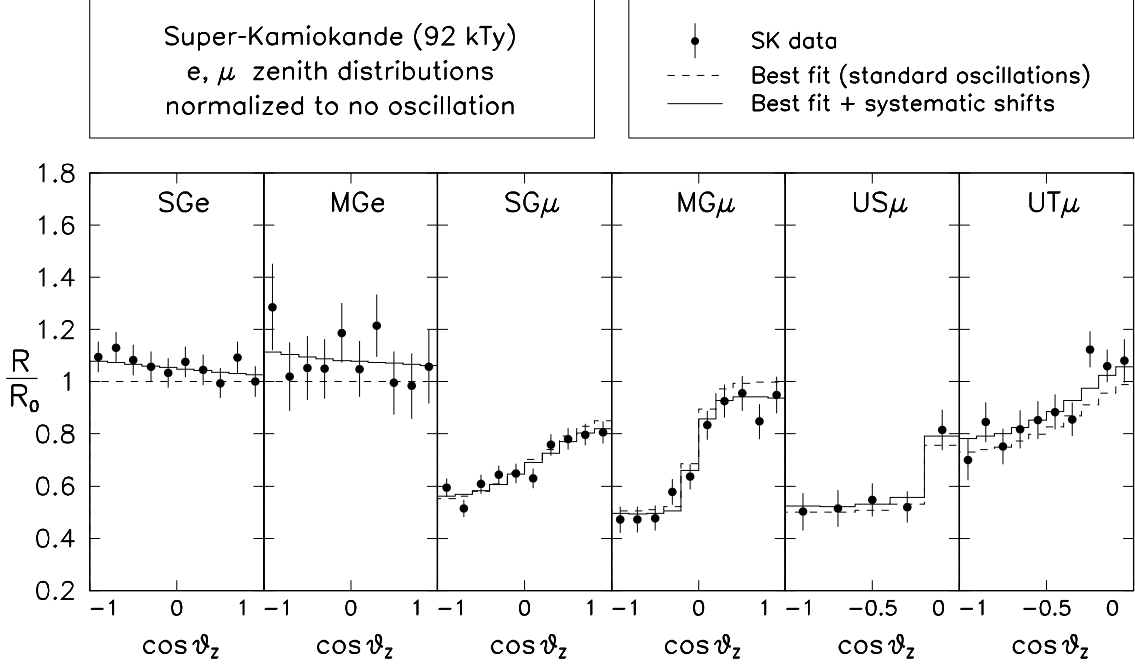


FIG. 4: Standard oscillations in the ν_e channel: SK experimental zenith distributions (1_{stat}), compared with the corresponding theoretical ones at the global (SK + K2K) best-fit point given in Table I. All distributions are normalized to the unoscillated predictions in each bin. For the theoretical event rates, we show both the central values R_n^{theo} (dashed histograms) and the “shifted” values \bar{R}_n^{theo} (solid histograms), which embed the effect of systematic pulls. The difference between \bar{R}_n^{theo} and R_n^{theo} shows how much (and in which direction) the correlated systematic errors tend to stretch the predictions in order to match the data. See the text and Appendix A for details.

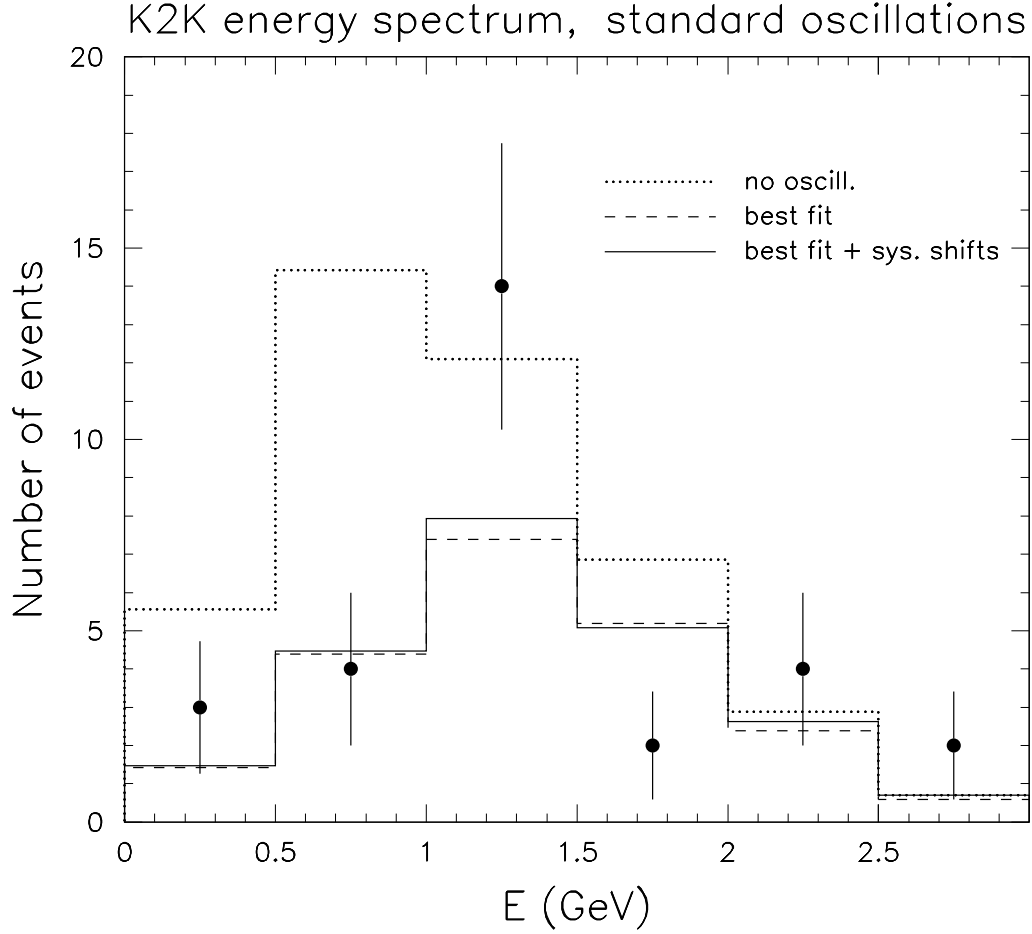


FIG. 5: Standard oscillations in the $\bar{\nu}_\mu \rightarrow \bar{\nu}_\tau$ channel: Absolute spectrum of (dominantly QE) events in K2K, as a function of the reconstructed neutrino energy E . The data points (29 events total) are shown as dots with 1_{stat} in each of the six bins. The dotted histogram represents our calculations for no oscillation. The solid and dashed histograms represent the theoretical predictions N_n^{theo} and N_n^{theo} at the global (SK + K2K) best-fit point in Table I, with and without systematic shifts, respectively. See the text and Appendix B for details.

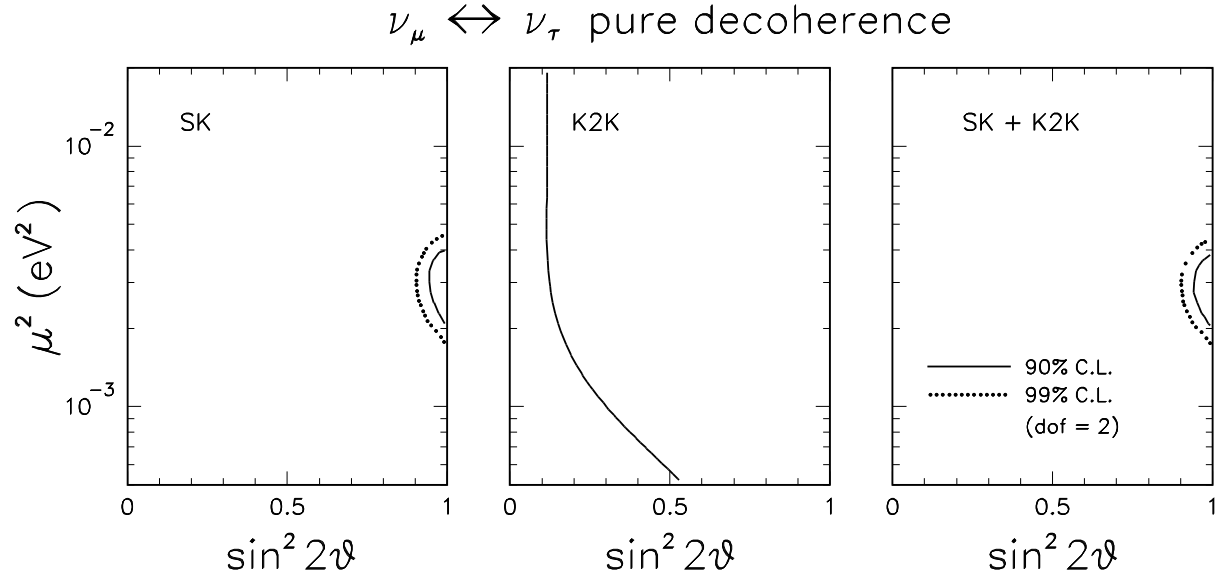


FIG. 6: As in Fig. 1, but for the pure decoherence scenario. Notice that the bounds on the $(\mu^2; \sin^2 2\vartheta)$ parameters are dominated by SK.

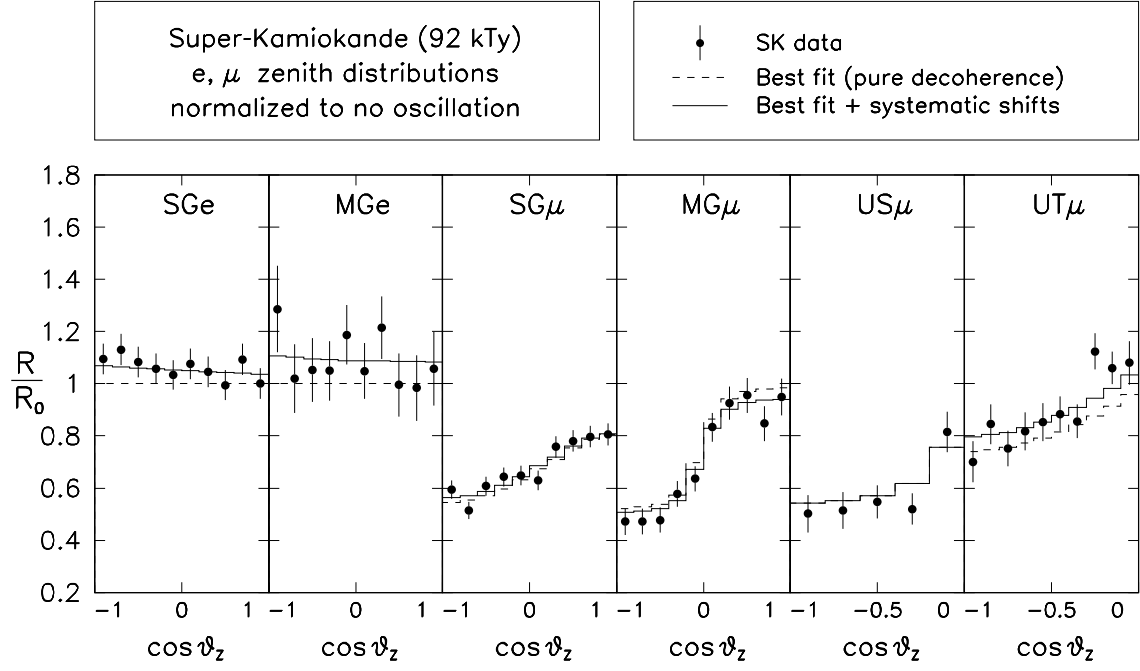


FIG .7: As in Fig.4, but for the global (SK + K2K) best- t point to the pure decoherence scenario, as given in Table I.

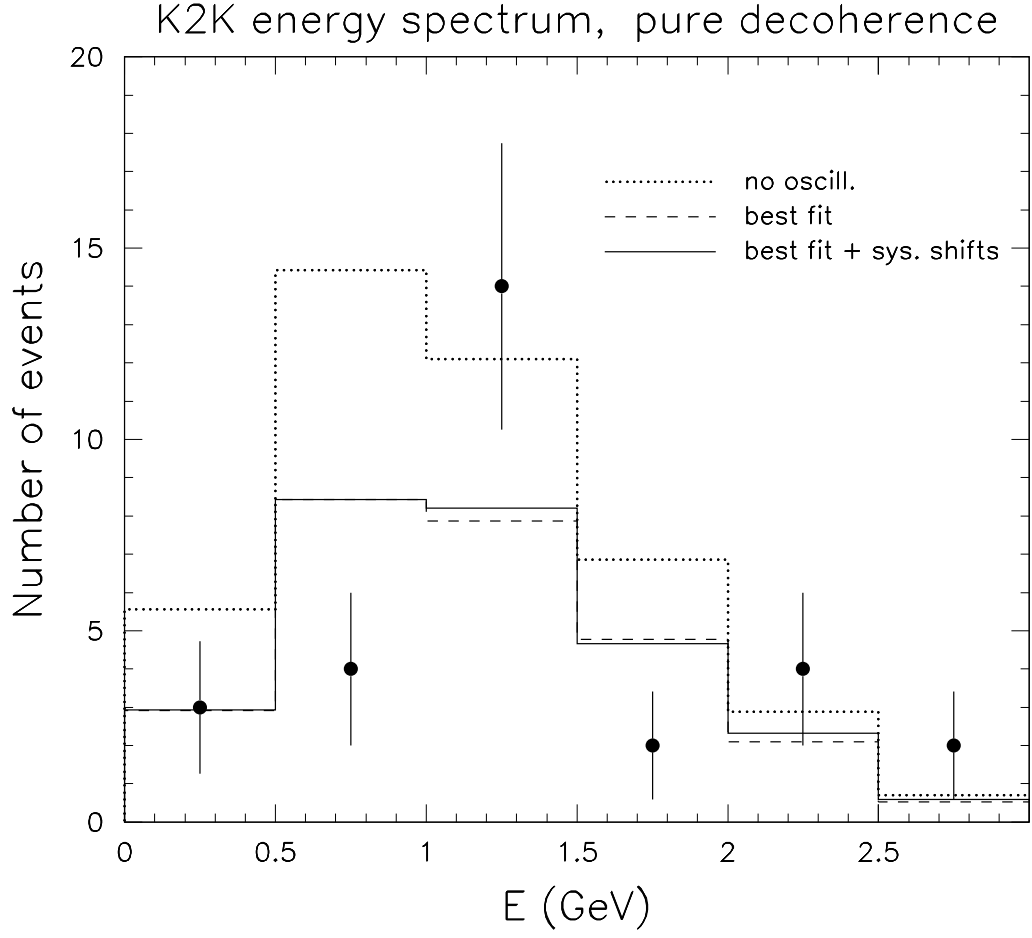


FIG .8: As in Fig.5, but for the global (SK + K2K) best-fit point to the pure decoherence scenario, as given in Table I.

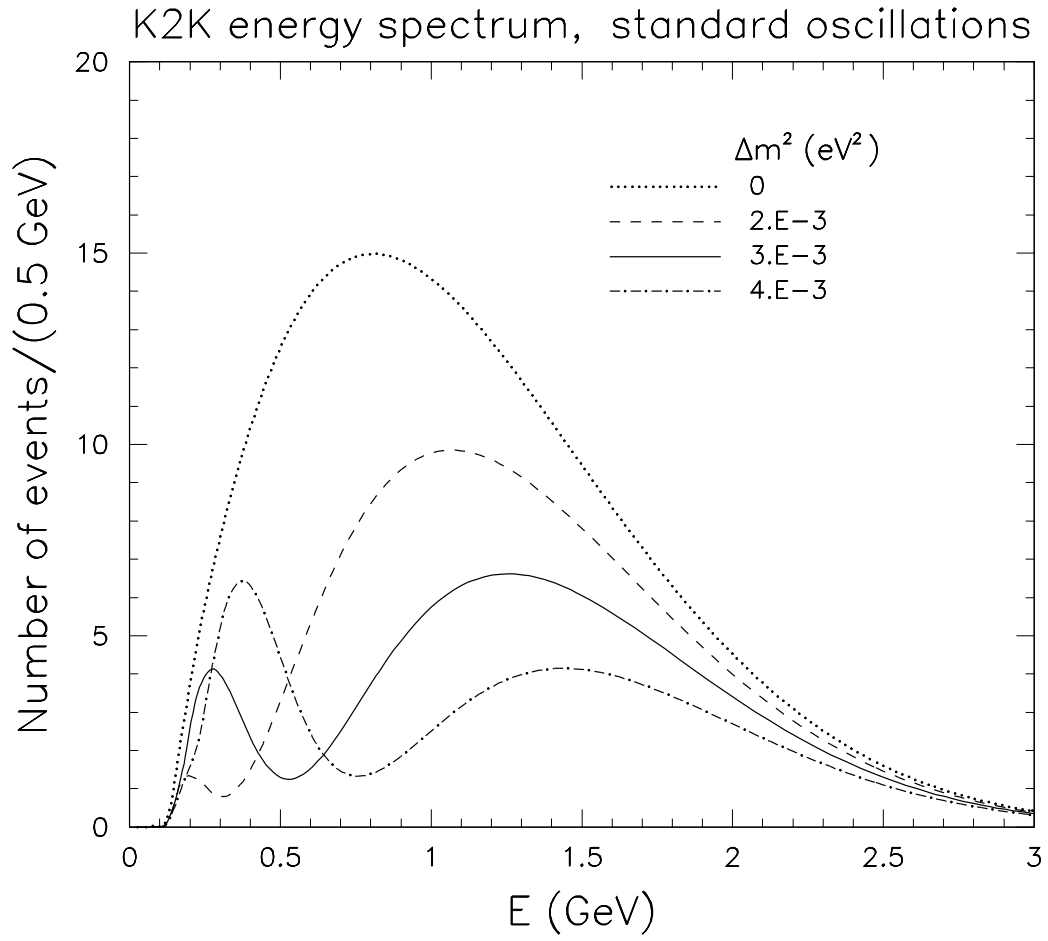


FIG. 9: Standard oscillations: Unbinned K2K theoretical spectrum at maximal mixing and for three representative values of m^2 .

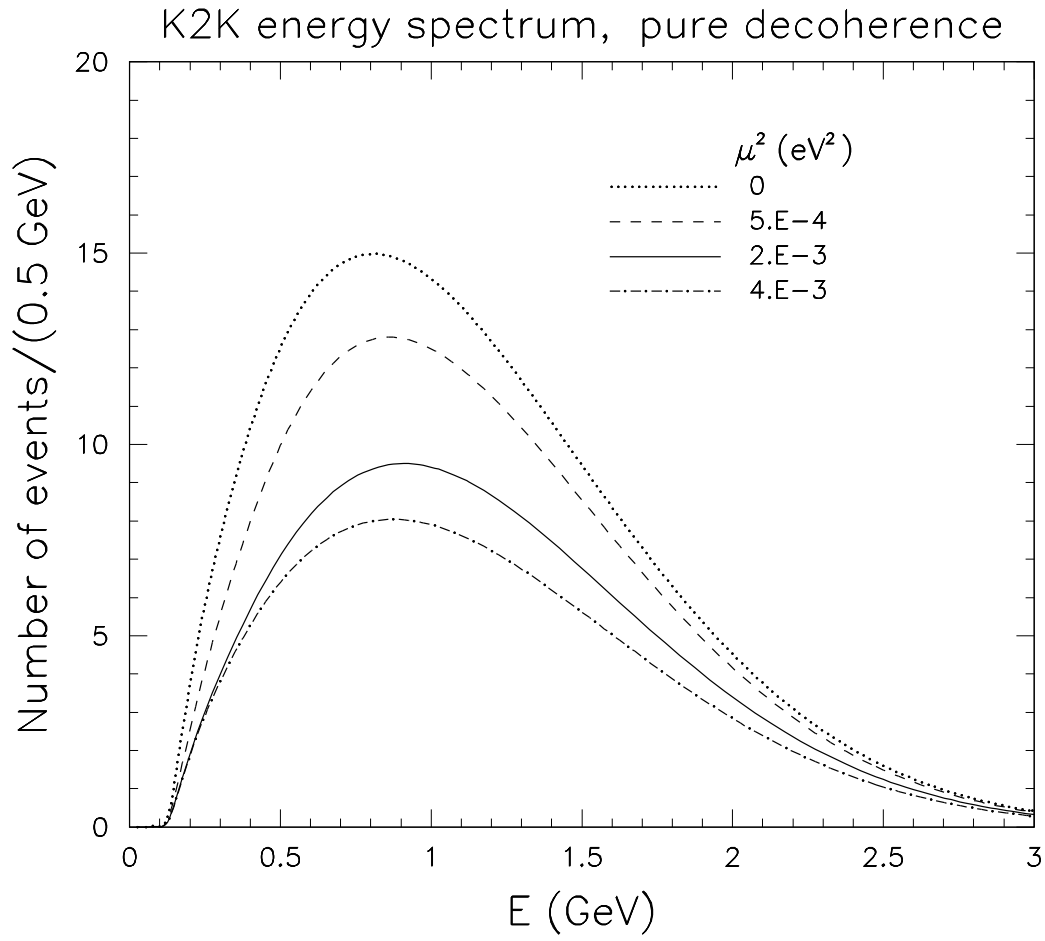


FIG .10: Pure decoherence: Unbinned K 2K theoretical spectrum at maximum mixing and for three representative values of μ^2 .

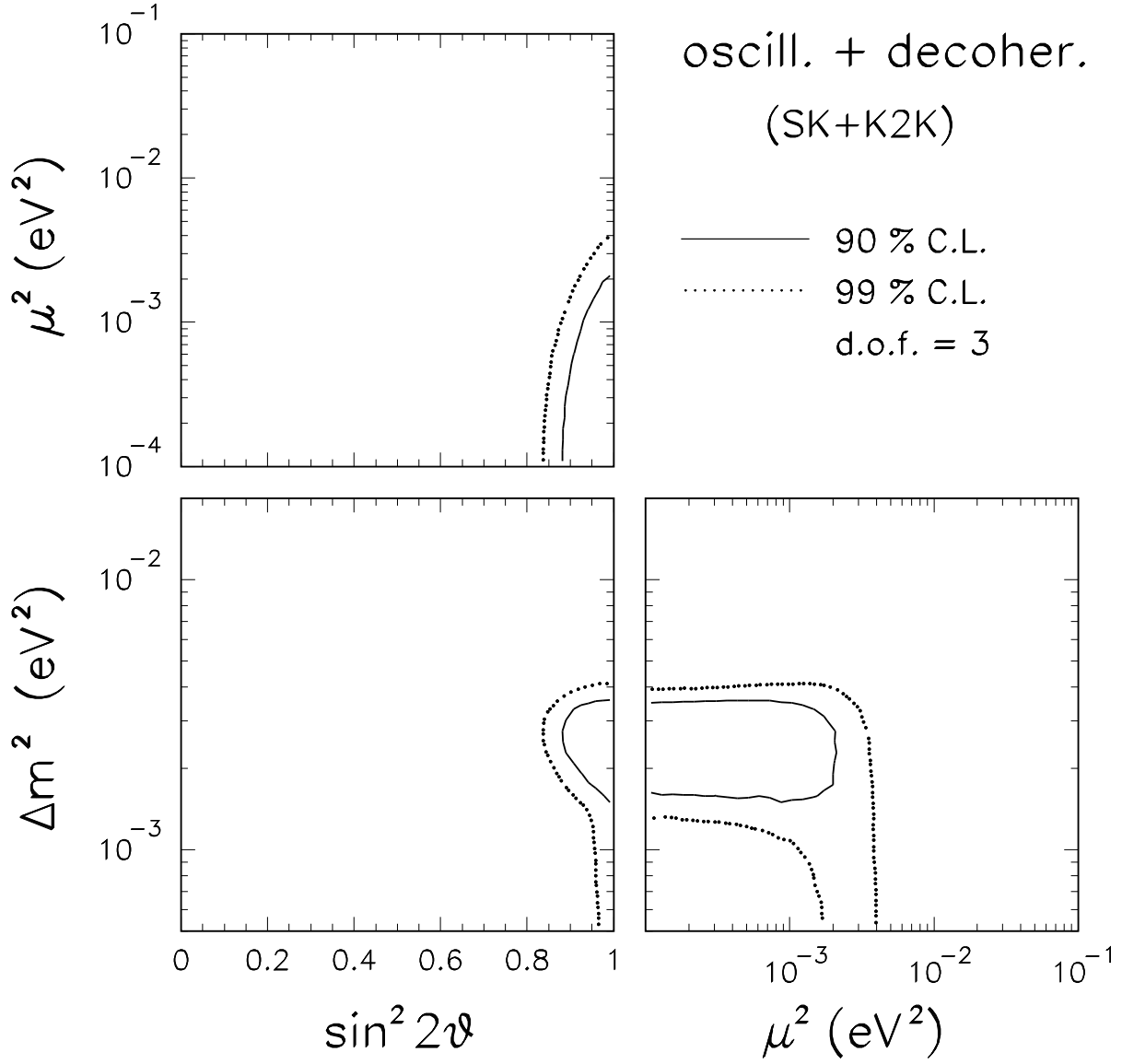


FIG. 11: General case (oscillations plus decoherence): Volume allowed by SK + K2K in the parameter space $(\mu^2; \sin^2 2\theta; \Delta m^2)$ at 90% and 99% C.L. for $N_{\text{DF}} = 3$ ($\chi^2 = 6.25$ and 11.34), shown through its projections onto the coordinate planes. The best-fit is reached in the limit of standard oscillations ($\Delta m^2 = 0$). However, the case of pure decoherence ($\mu^2 = 0$) is still marginally allowed. In all cases, the mixing is nearly maximal ($\sin^2 2\theta \rightarrow 1$)

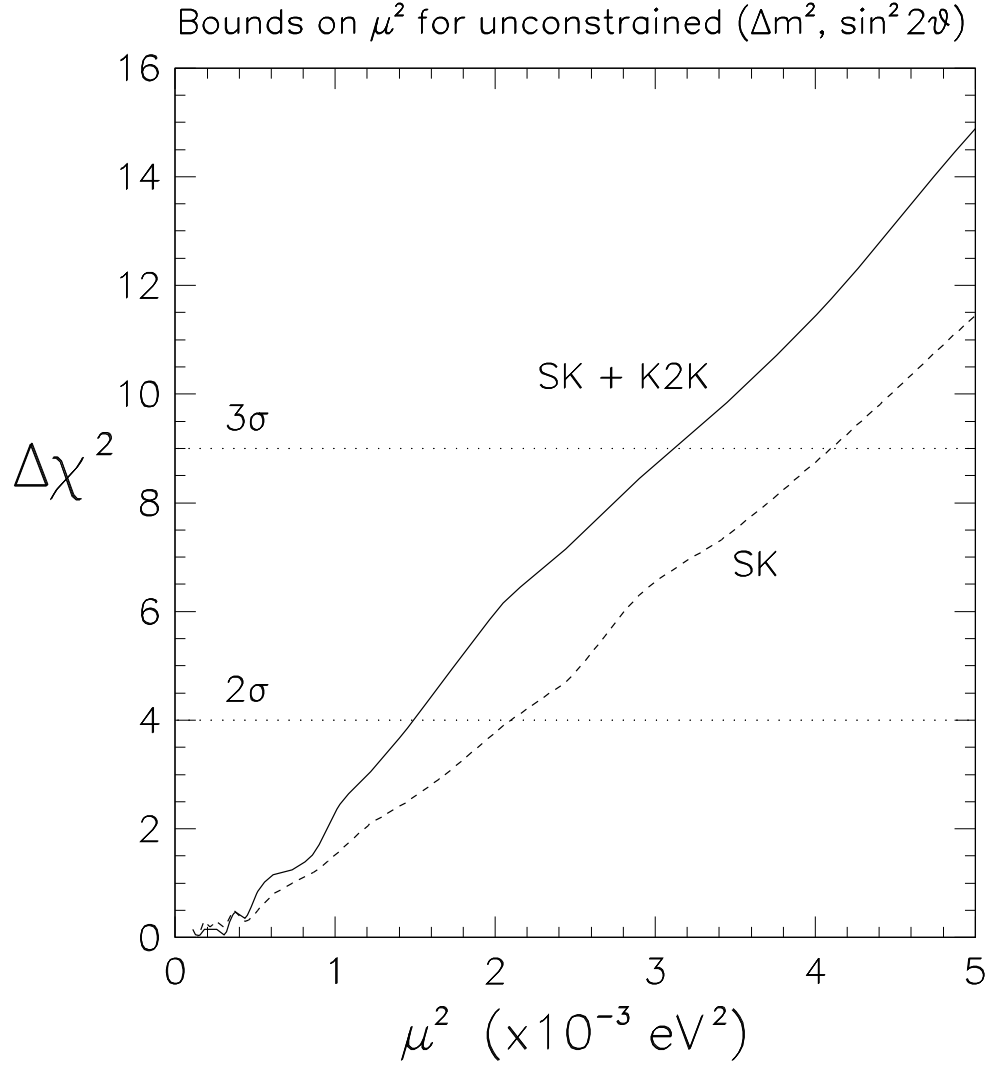


FIG. 12: General case (oscillations plus decoherence): Upper bounds on the decoherence parameter $\Delta\chi^2$, for unconstrained $(\Delta m^2; \sin^2 2\vartheta)$. The intersections with the horizontal dotted lines give the 2 and 3 upper bounds on $\Delta\chi^2$ for $N_{DF} = 1$.